X-point tunneling in AlAs–GaAs–AlAs double barrier heterostructures

D. Z.-Y. Ting and T. C. McGill
Thomas J. Watson, Sr. Laboratory of Applied Physics, California Institute of Technology, Pasadena, California 91125

(Received 7 April 1989; accepted 14 April 1989)

The dynamics of X-point tunneling in AlAs–GaAs–AlAs double barrier heterostructures is studied with numerical simulation. The problem is formulated within the framework of the one-band Wannier orbital model which allows for simultaneous descriptions of the Γ-point double barrier profile and the X-point double well profile in this heterostructure. Time dependences of the following processes are illustrated: (i) resonant tunneling of Γ-valley electron packets via the X-point quantum well states localized in the AlAs layers, (ii) nonresonant tunneling of Γ-electron packets (with energy below the AlAs Γ-point barrier) through the X-point continuum states, and (3) resonant tunneling via Γ-X mixed quantum well states localized in both the GaAs Γ-point quantum well and the AlAs X-point double quantum well. In addition, the effects of X-point tunneling on the escape times of electrons localized in the GaAs quantum wells are examined.

I. INTRODUCTION

Negative differential resistance (NDR) in resonant tunneling double barrier heterostructures (DBH) was originally proposed by Tsu and Esaki,[1] and first observed experimentally by Chang *et al.*[2] More recently, high-quality samples of DBH have also been shown to exhibit large peak-to-valley ratios.[3–5] Because of its technological importance, resonant tunneling in heterostructures has been the subject of intense theoretical and experimental investigation. While the bulk of the theoretical work on resonant tunneling has been based upon the time-independent Schrödinger equation, a number of results have been obtained involving numerical solution of the time-dependent Schrödinger equation.[6–10] Since the exact nature of the resonant tunneling process has been a subject of some controversy,[11–16] and the interpretation of resonant tunneling time has also been under extensive debate,[17] numerical simulation has proven to be a valuable tool. Harada and Kuroda[6] have used simulation to verify that tunneling time is related to the transmission resonance width. Collins, Lowe, and Barker have used numerical results to help clarify the concept of tunneling time,[17] and to establish a criterion for distinguishing hopping tunneling from true resonant tunneling.[9]

In this paper we present a numerical study of the dynamics of tunneling processes in the AlAs–GaAs–AlAs double barrier heterostructures. Unlike previous simulation studies, which make use of the effective mass approximation, we have incorporated realistic band structure effects in our model. This approach allows us to study X-point tunneling processes in double barriers; experimental observations[18] indicate that these processes can be of considerable importance. To help clarify what we mean by X-point tunneling, in Fig. 1(a) we plot the lowest conduction band of bulk GaAs and AlAs along [001]. We have assumed that 70% of the direct band gap difference between AlAs and GaAs is associated with the conduction band. Note that the AlAs X-point energy is lower than that of GaAs. In Fig. 1(b) we plot the Γ-point and X-point energies as functions of position along the growth direction for a (001) AlAs–GaAs–AlAs DBH. Note that while the Γ-profile exhibits the familiar double barrier structure, the X-point profile shows a double-well structure instead. Like the Γ-point double barrier, the X-point double well has its own associated resonant levels which are accessible to tunneling electrons. The emphasis of this paper will be on tunneling processes involving the X-point states. In Sec. II we briefly describe the method used in our simulation. In Sec. III we present our results on tunneling of Gaussian packets and tunneling escape times. The summary is given in Sec. IV.

II. METHODS

We include band structure effects in our simulation using the one-band Wannier orbital model (OBWOM).[19] In

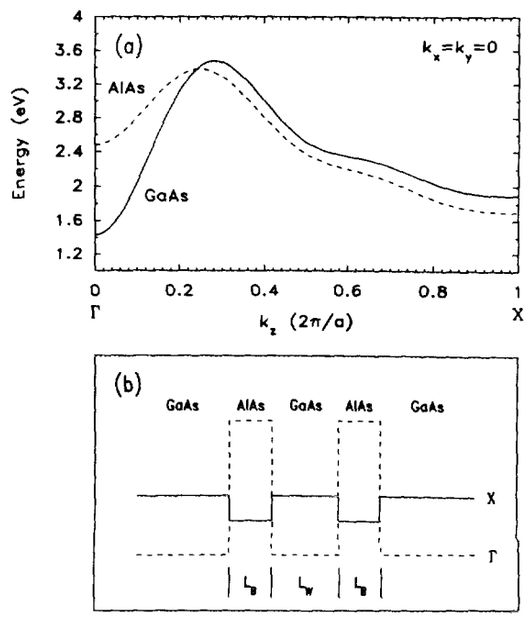

FIG. 1. (a) The lowest conduction band in GaAs and AlAs along the [001] direction. (b) (001) AlAs–GaAs–AlAs DBH conduction band edge profile at the Γ-point and the X-point.

 0734-211X/89/041031-04$01.00

OBWOM only one orbital per unit cell is used. Each orbital is allowed to interact with many neighbors to produce a band structure corresponding to the lowest conduction band that is accurate over the entire Brillouin zone. The band structures shown in Fig. 1(a) are produced by OBWOM. Using the Wannier orbitals we can form planar orbitals by taking Bloch sums over all orbitals in a lattice plane perpendicular to the growth direction. GaAs and AlAs planar orbitals are used to construct the DBH used in our simulation. In the simulation, an initial wave function placed on the sample is propagated in time by solving the time-dependent Schrödinger equation.

The total number of planes, or monolayers, used to simulate the device is limited by the available computational resources. In our case, we use a sample size of 1000 monolayers. Ideally, the sample size should be large enough so that as the wave function evolves in the time period of interest, it does not reach the sample boundaries at which reflections occur. However, for resonant tunneling processes, the time period of interest can be quite long[12] so that a computationally practical sample size is not sufficient to satisfy that condition. Rather than letting the outgoing waves reflect back,[8] we devised a scheme to simulate absorbing boundaries. We set aside regions of ~100 monolayers at each end of the sample as the absorbing layers. We then evolve the wave function for a small time step, and at the end of each time step attenuate the wave function in the absorbing layers. We found empirically that if we used a smooth cutoff, i.e., if we let the wave function in the absorbing layers decrease smoothly to zero, and chose a time step appropriate to the wave velocity and absorbing layer thickness, boundary reflections are virtually eliminated.

III. RESULTS AND DISCUSSION

In Part A of this section, we examine the qualitative features of X-point tunneling by studying tunneling of Gaussian packets through double barrier heterostructures. In Part B, we examine the effect of X-point tunneling on the tunneling escape rates of electrons from double barrier heterostructure quantum wells.

A. Tunneling of Gaussian packets

We consider tunneling of Gaussian packets through symmetric double barrier heterostructures for selected examples. In each of the simulation samples, we let the well be L_W monolayers of GaAs, and each of the barriers be L_B monolayers of AlAs. The left electrode consists of 700 layers of GaAs, and the right electrode consists of $(300 - L_W - 2L_B)$ layers of GaAs. We let the initial Gaussian packet be centered at 401 monolayers from the left boundary. The packet width is chosen to be 102 monolayers, corresponding to 0.0022 $2\pi/a$ in k-space. The tails of the Gaussian packet are truncated so that there is no amplitude in the device region initially. The center of the Gaussian packet in k-space is located in the Γ-valley, so that the initial packet is a linear combination of GaAs Γ electron states only.

In the first example, we examine a structure with $L_W = 5$ and $L_B = 5$ in which the lowest quasi-bound states are X-like states localized in the AlAs (barrier) layers. The packet energy is chosen to match the energy of the lowest quasi-bound state, above the GaAs X-point energy but below the AlAs X-point energy. Figure 2 shows the probability density in the device region as a function of time displayed as a grey-scale contour plot. The darker areas in the contour plot indicate regions of higher probability density. Note that the probability density builds up in the first barrier and then slowly decays, indicating that the incoming Γ electron is scattered into the X-valley in the AlAs barrier. However, if we monitor the transmitted wave function, we find that it consists predominantly of Γ-valley components. In addition, we find that the total probability in the right electrode builds up slowly, as is characteristic of a resonant tunneling process.

In the second example we use the same structure as in the previous example, but with a packet energy 12 meV above the AlAs X-point level, which is in the energy range of the continuum X-states (but still far below the continuum Γ states). The resulting probability density plot is shown in Fig. 3. Unlike the previous example, in which tunneling takes place over an extended period, transmission here is essentially complete after 125 fs, indicating a fast, nonresonant tunneling process. However, note that while a portion of the transmitted electron probability density quickly moves away from the device, a significant amount remains trapped in the region just outside the right AlAs barrier. Eventually, the trapped component moves away from the device, but the time scale for this process is considerably longer than for ordinary Γ-point nonresonant tunneling. Careful examination of the Fourier transform of the transmitted wave reveals that both Γ-valley and X-valley components are present. The Γ-valley component we recognize as the fast component which has undergone Γ-point nonresonant tunneling. The X-valley component is the part that moves away slowly due to the large X-point effective mass.

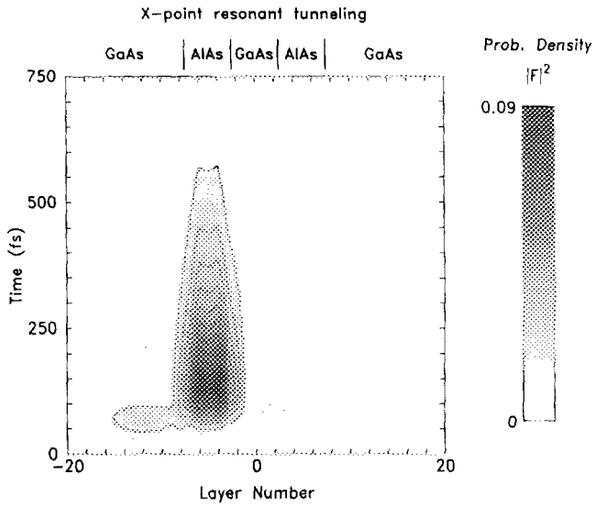

FIG. 2. Probability density as a function of time in the region around a DBH during an X-point resonant tunneling process. The DBH structure is $L_W = 5$ and $L_B = 5$. The Gaussian packet energy is 1.7532 eV.

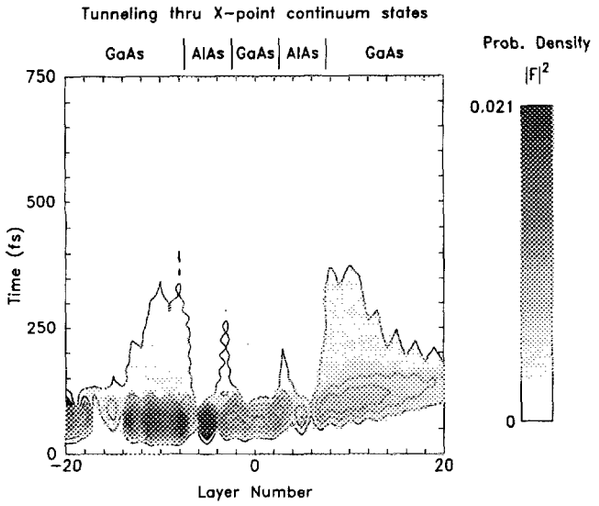

FIG. 3. Probability density as a function of time in the region around a DBH during a tunneling process involving continuum X-states. The DBH structure is $L_W = 5$ and $L_B = 5$. The Gaussian packet energy is 1.9120 eV.

The third example is a double barrier structure with $L_W = 9$ and $L_B = 5$. For this structure, the lowest quasibound state is a Γ–X mixed level which has large amplitudes in the GaAs well region and the two AlAs barrier regions. This is of considerable interest since Γ–X mixing has recently been observed in GaAs/AlAs superlattices.[20] As in the first example, we pick the packet energy to match the energy of the lowest quasibound state. The resulting probability density as a function of time is shown in Fig. 4. Note that there is significant buildup of probability density in the two barriers and the well during the tunneling process. An interesting effect in this structure is the oscillation of the probability density between the two barrier region. Note that this oscillation is very rapid, occuring with a period of ~ 200 fs. The Fourier transform of the transmitted wave shows that it

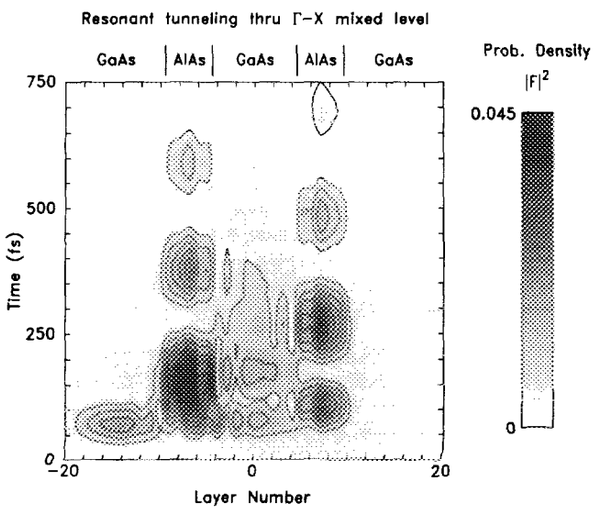

FIG. 4. Probability density as a function of time in the region around a DBH during a tunneling process through a Γ–X mixed level. The DBH structure is $L_W = 9$ and $L_B = 5$. The Gaussian packet energy is 1.7715 eV.

consists predominantly of Γ-valley components. However, unlike in normal Γ-point resonant tunneling where the probability density is transmitted in a steady stream, the transmitted wave in this case is generated in pulses. The timing of the generation of the pulses coincided with the build-up of probability density in the right barrier.

B. Escape from quantum well

Having discussed some qualitative features of X-point tunneling, in this subsection we examine its effect on the tunneling escape rates from DBH quantum wells. Fast electron tunneling escape times from quantum well in DBH have been measured recently.[21,22] In our simulation of the tunneling escape process, we choose the initial wave function to be a rectangular pulse localized in the GaAs quantum well. By monitoring the probability density in the device region as a function of time, we can extract the escape time. We have tested the simulation with other initial wave function shapes (i.e., half-sine), and found that while the transient response is different, the steady-state behavior from which we extract the tunneling time is essentially the same.

We examined a series of symmetric double barrier heterostructures, all with barrier width $L_B = 13$, but with well widths ranging from $L_W = 5$ to $L_W = 15$. We plot the quasibound state energy levels as functions of well width in Fig. 5. Note that for $L_W > 10$, the lowest quasi-bound level is a Γ state localized in the GaAs quantum well. This is the familiar situation in which the effective mass approximation applies. For $L_W \leqslant 10$, we expect effects due to the presence of X states to become important. Note that we do not find any Γ quasibound states for the ultra thin well cases of $L_W = 5$ and $L_W = 6$.

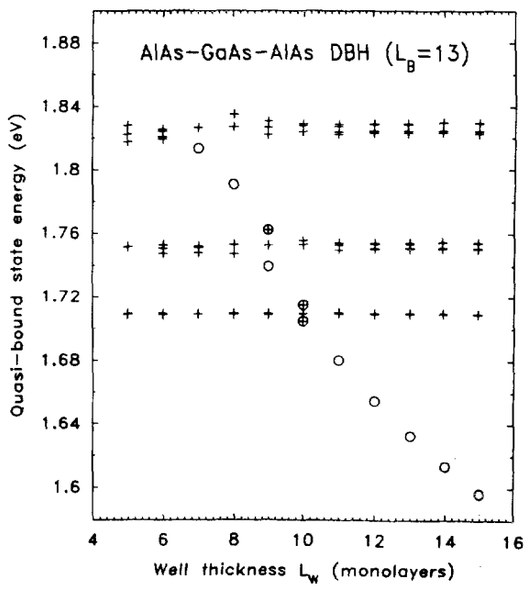

FIG. 5. Quasibound state energy levels of symmetric DBH with barrier width $L_B = 13$ for various well widths L_W. Energy is measured from the GaAs valence-band edge. Circles and crosses indicate the states with significant probability density of being found in the GaAs well and in the AlAs barriers, respectively.

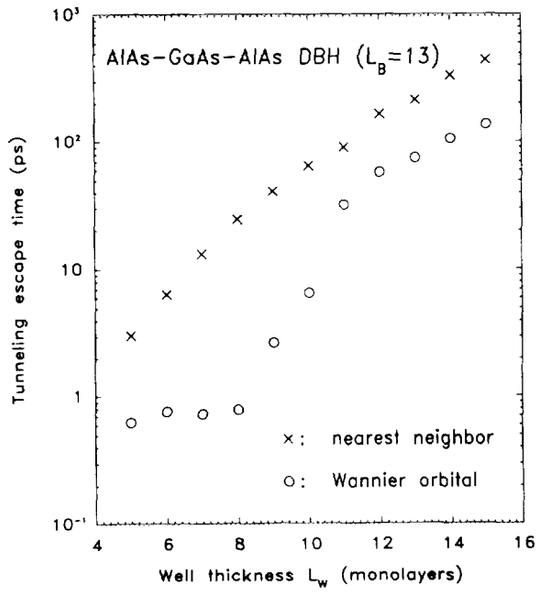

FIG. 6. Tunneling escape times for symmetric double barrier heterostructure as a function of L_W, with $L_B = 13$.

In Fig. 6 we plot the tunneling escape time as a function of well width. For comparison with the times obtained by simulation using the one-band Wannier orbital model, we have included in the same figure tunneling times for a one-band model in which only the nearest-neighbor interaction is used. The nearst-neighbor model parameters are chosen to yield a band struture which has the correct Γ-valley effective mass; there are no X-valleys in this model. In the energy range under consideration, the nearest-neighbor model yields the same quasi-bound states as the effective mass approximation. Note that for $L_W \geqslant 11$, the Wannier orbital model yields the same trend as the nearest-neighbor model. For $L_W = 9$ and $L_W = 10$, the Wannier orbital model times decrease much faster with the well width than the nearest-neighbor model predicts. For $L_W \leqslant 8$, the Wannier orbital model escape times are nearly independent of L_W. If we examine the wave function in the electrodes (i.e., the part of the wave function that has escaped) for the three regimes described above, we find that they are qualitatively very different. For $L_W \geqslant 11$, where the lowest quasi-bound state is a Γ state, the wave function escapes in a steady stream into the Γ-valley. For $L_W = 9$ and $L_W = 10$, where the lowest Γ quasibound state is comparable in energy to the lowest X quasibound states, the wave function escapes predominantly as pulses into the Γ-valley, reminiscent of the Γ–X mixed level resonant tunneling example described previously. And for $L_W \leqslant 8$, where the Γ quasibound states are high in energy compared to the lowest X quasibound states, a significant portion of the wave function escapes into the X-valley.

IV. SUMMARY AND CONCLUSIONS

We have studied X-point tunneling in AlAs–GaAs–AlAs double barrier heterostructures using a numerical simulation technique which allows us to take the band-structure effects into consideration. We find that band-structure effects are responsible for processes that cannot be accounted for in simple effective mass models, including X-point resonant tunneling, non-resonant tunneling via X-point continuum states, and resonant tunneling through Γ–X, mixed quasi-bound states. Depending on the circumstances, a Γ-valley electron packet tunneling through X-point states can be transmitted into either the Γ- or the X-valley. We have also studied tunneling escape rates in AlAs–GaAs–AlAs double barrier heterostructures. It is found that in structures with narrow well widths, in which the lowest quasibound states are X states, X-point tunneling can play a significant role in determining the tunneling escape times from the quantum well.

ACKNOWLEDGMENTS

The authors would like to thank M. K. Jackson, D. H. Chow, and E. T. Yu for helpful discussions. This work is supported by the U. S. Office of Naval Research (ONR) under Grant No. N00014-89-J-1141.

[1] R. Tsu and L. Esaki, Appl. Phys. Lett. **22**, 562 (1973).
[2] L. L. Chang, L. Esaki, and R. Tsu, Appl. Phys. Lett. **24**, 593 (1974).
[3] T. C. L. G. Sollner, W. D. Goodhue, P. E. Tannenwald, C. D. Parker, and D. D. Peck, Appl. Phys. Lett. **43**, 588 (1983).
[4] T. C. L. G. Sollner, P. E. Tannenwald, D. D. Peck, and W. D. Goodhue, Appl. Phys. Lett. **45**, 1319 (1984).
[5] C. I. Huang, M. J. Paulus, C. A. Bozada, S. C. Dudley, K. R. Evans, C. E. Stutz *et al.*, Appl. Phys. Lett. **51**, 121 (1987).
[6] N. Harada and S. Kuroda, Jpn. J. Appl. Phys. **25**, L871 (1986).
[7] B. Jogai, K. L. Wang, and K. W. Brown, J. Appl. Phys. **59**, 2968 (1986); Superlattices and Microstructures **2**, 259 (1986).
[8] A. P. Jauho and M. M. Nieto, Superlattices and Microstructures **2**, 407 (1986).
[9] S. Collins, D. Lowe, and J. R. Barker, J. Phys. C **20**, 6233 (1987).
[10] R. G. Hay, T. B. Bahder, and J. D. Bruno, SPIE **943**, Quantum Well and Superlattice Phys. II, 22 (1988).
[11] M. O. Vassell, J. Lee, and H. F. Lockwood, J. Appl. Phys. **54**, 5206 (1983).
[12] B. Ricco and M. Ya. Azbel, Phys. Rev. B **29**, 1970 (1984).
[13] S. Luryi, Appl. Phys. Lett. **47**, 490 (1985).
[14] T. Weil and B. Vinter, Appl. Phys. Lett. **50**, 1281 (1987).
[15] M. Büttiker and R. Landauer, Phys. Rev. Lett. **49**, 1739 (1982).
[16] M. Büttiker, IBM J. Res. Dev. **32**, 63 (1988).
[17] For a review of the issue, see, for example, S. Collins, D. Lowe, and J. R. Barker, J. Phys. C **20**, 6213 (1987).
[18] E. E. Mendez, E. Calleja, C. E. T. Gonçalves da Silva, L. L. Chang, and W. I. Wang, Phys. Rev. B **33**, 7368 (1986); Appl. Phys. Lett. **50**, 1263 (1987).
[19] D. Z.-Y. Ting and Y. C. Chang, Phys. Rev. B **36**, 4357 (1987).
[20] M.-H. Meynadier, R. E. Nahory, J. M. Worlock, M. C. Tamargo, J. L. de Miguel, and M. D. Sturge, Phys. Rev. Lett. **60**, 1338 (1988).
[21] M. Tsuchiya, T. Matsusue, and H. Sakaki, Phys. Rev. Lett. **59**, 2356 (1987).
[22] M. K. Jackson, M. B. Johnson, D. H. Chow, T. C. McGill, and C. W. Nieh, Appl. Phys. Lett. **54**, 552 (1989).